Zeitschrift: IABSE publications = Mémoires AIPC = IVBH Abhandlungen
Band: 35 (1975)

Artikel: Lateral buckling strength of plate girders
Autor: Yoshida, H.
DOI: https://doi.org/10.5169/seals-26952

Lateral Buckling Strength of Plate Girders

Tension de flambage latéral de poutres à âme pleine

Kippwiderstand von Vollwandträgern

H. YOSHIDA
Associate Professor of Civil Engineering
Kanazawa University, Kanazawa, Japan

Introduction

The lateral buckling strength of beams in the elastic and the inelastic range is governed by the flexural rigidity about the weak axis, St. Venant torsional rigidity and the warping rigidity of the cross section. The contributions of these rigidity of the elastic buckling strength are quite different for the compact section with large span length and for the thin-walled section with short span [1]. In the inelastic range, the problem is more complicate because the amount of yielding, and therefore the rigidities of the beam for the buckling, is dependent upon the applied critical moment. Even for I-shaped cross section usually used in structures, the direct relationship between the geometrical dimensions of the cross sections and the lateral buckling strength has not yet been established generally in the inelastic range.

First attempt to consider the effects of residual stresses was made by GALAMBOS [4] and he suggested an approximate method applicable to the lateral buckling of beams with general wide-flange cross sections under uniform moment. Nethercot also proposed an approximate design formula [11] in the inelastic range who investigated the various factors affecting the inelastic lateral buckling of beams. These formulae were inductively introduced from several typical cross sectional dimensions and thus the factors of the cross sectional dimensions affecting the lateral buckling of beams are not clear.

In this paper, the lateral buckling strength on the elastic and the inelastic ranges will be discussed for the I-shaped plate girders of which dimensions are with the thin web comparing with the flange thickness. For the plate girders with such dimensions, it will be shown that the lateral buckling strength can be expressed by only the ratio of the depth of the cross section to the web height with respect to the cross sectional geometry in both the elastic and the inelastic ranges and also the influence of such factors as cross sectional geometry, loading conditions, yield stress levels and residual stress distributions will be discussed in a general form.

Futhermore, the effect of the variations of cross sections with tapering flange widths or web depths on the elastic and the inelastic lateral buckling will be investigated.

Assumptions

The assumptions associated with the analysis are as follows:

1. The cross section of the plate girders is I-shaped doubly symmetric and the geometric center is horizontal and straight.
2. The effects of the web to the lateral flexural rigidity and the warping rigidity may be neglected and even to the St. Venant torsional rigidity may be neglected since $d_w w^3/2bt^3$ is less than 6% for the I-shaped plate girders usually used, in which d_w = the web height; w = the web thickness; b = the flange width and t = the flange thickness (see Fig. 1a). Furthermore, since after yielding of both flanges of I-shaped plate girders, the carrying capacity can not be expected, this assumption may be allowable.
3. The plate girders are perfectly straight before the buckling occurs and the cross section does not distort before and after the buckling.
4. The vertical displacement is small.
5. The stress-strain relation is for the elastic-perfectly-plastic.
6. The residual stress in the cross section distributes in the flanges only. The distribution of the residual stress is symmetric about axes of symmetry of the cross section. The residual stress in a cross section is in self-equilibrium and are ideally assumed as Figs. 1b and c for as-rolled and as-welded shapes, respectively.
7. The stiffnesses of lateral bending and warping in the inelastic range are calculated by the tangent modulus theory. The stiffness of the St. Venant torsion is by the incremental theory which predicts the same St. Venant torsional stiffness for the yielded portion as that of the elastic portion.
8. The variation of a cross section is not so steep that the assumptions associated with the so-called beam theory can not be available.

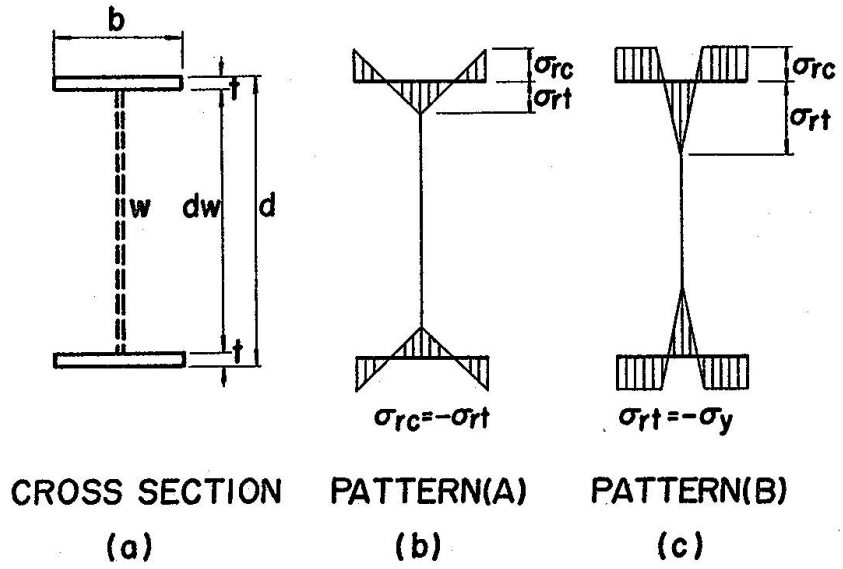

Fig. 1. Simplified cross section and idealized residual stresses.

As shown in Fig. 2, the x and y coordinates of the centroid of a small rectangular element in a flange divided by the horizontal and the vertical lines may be expressed by ξb and ηd of which origin locates at the center of the cross section, in which d = the depth of the cross section. The strain, ε, at the centroid of the element is the combination of the strain, ε_ϕ, due to the bending which is proportional to the distance from the center of the cross section, the strain, ε_o, which yields uniformly on the whole cross section and the strain, ε_r, due to the residual stress.

$$\varepsilon = \varepsilon_\phi + \varepsilon_o + \varepsilon_r = 2\varepsilon_y\left(\frac{\phi}{\phi_y}\right)\eta + \varepsilon_o + \varepsilon_r \tag{1}$$

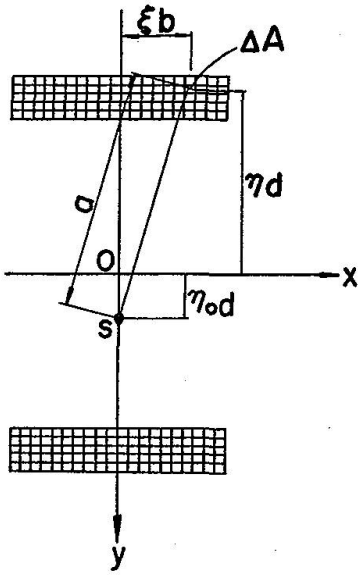

Fig. 2. Subdivided cross section.

in which ε_y = the strain corresponding to the yield stress; ϕ = the curvature and ϕ_y = the curvature corresponding to the yield in flexure.

Thus, the stress, σ, at the centroid of a small rectangular element becomes

$$\begin{aligned} \sigma &= E\varepsilon && |\varepsilon| \leqq \varepsilon_y \\ \sigma &= \sigma_y \cdot \mathrm{sgn}(\varepsilon) && |\varepsilon| > \varepsilon_y \end{aligned} \tag{2}$$

in which E = Young's modulus of elasticity; σ_y = the yield stress; $\mathrm{sgn}(\varepsilon) = 1.0$ when ε is positive and $\mathrm{sgn}(\varepsilon) = -1.0$ when ε is negative. From the equilibrium of longitudinal direction, $\int_A \sigma dA = 0$,

$$\sum_E \left(\frac{\varepsilon}{\varepsilon_y}\right) + \sum_P \mathrm{sgn}\left(\frac{\varepsilon}{\varepsilon_y}\right) = 0 \tag{3}$$

must be satisfied in which $\sum_E$ means the sum for the elastic elements only and $\sum_P$ means the sum for the yielded elements.

By the trial and error procedure, the strain, ε_o, in Eq. 1 which is satisfied by Eq. 3 can be obtained for a given curvature, ϕ/ϕ_y. Then, the strain and the stress at the centroid of the small rectangular element can be known.

The bending moment corresponding to the curvature, ϕ/ϕ_y, is

$$\frac{M}{M_y}=\frac{3}{mn(1+\beta+\beta^2)}\left\{\sum_E\left(\frac{\varepsilon}{\varepsilon_y}\right)\cdot\eta+\sum_P\mathrm{sgn}\left(\frac{\varepsilon}{\varepsilon_y}\right)\cdot\eta\right\} \tag{4}$$

in which m and n = the subdivided numbers of the flange thickness and the flange width with equal intervals, respectively; M_y = the yield moment without residual stress and $\beta=d_w/d$, the ratio of the web height, d_w, to the depth of the cross section, d.

The moment of inertia about the weak axis, I_y, and the warping moment of inertia, I_w, for the elastic core of the cross section corresponding to M/M_y are given by

$$I_y=\mu_{iy}\kappa_{iy}b^3d \tag{5a}$$

$$I_w=\mu_{iw}\kappa_{iw}b^3d^3 \tag{5b}$$

The equivalent St. Venant torsional stiffness, $G\bar{K}_T$, defined by the combination of the St. Venant torsional stiffness, GK_T, and the contribution to the torque caused by the normal stress, $\int_A\sigma a^2dA$, and the section modulus about the strong axis, S, are given by

$$G\bar{K}_T=GK_T+\int_A\sigma a^2dA=\mu_{kt}\kappa_{kt}bd^3 \tag{6a}$$

$$S=\mu_s bd^2 \tag{6b}$$

in which a = the distance between the point on a flange and the shear center, μ's in Eqs. 5 and 6 are functions with respect to only β defined by

$$\mu_{iy}=\tfrac{1}{12}(1-\beta) \tag{7a}$$

$$\mu_{iw}=\tfrac{1}{192}(1-\beta)(1+\beta)^3 \tag{7b}$$

$$\mu_{kt}=\tfrac{1}{12}(1-\beta)^2 \tag{7c}$$

$$\mu_s=\tfrac{1}{6}(1-\beta^3) \tag{7d}$$

and κ's are the reduction factors for the coefficients in the inelastic range given by

$$\kappa_{iy}=\frac{6}{mn}\sum_E\xi^2$$

$$\kappa_{iw}=\frac{6}{mn}\frac{\sum_{Eu}\zeta^2\sum_{El}\zeta^2}{\sum_E\zeta^2}\left\{\frac{\sum_{Eu}\zeta^2\eta}{\sum_{Eu}\zeta^2}-\frac{\sum_{El}\zeta^2\eta}{\sum_{El}\zeta^2}\right\} \tag{8a}$$

$$\kappa_{kt}=1.0-\frac{6}{mn(1+\beta+\beta^2)}\bar{\nu}\varepsilon_y\left[\left\{\sum_E\left(\frac{\varepsilon}{\varepsilon_y}\right)(\eta-\eta_o)^2+\sum_P\mathrm{sgn}\left(\frac{\varepsilon}{\varepsilon_y}\right)(\eta-\eta_o)^2\right.\right. \tag{8b}$$

$$\left.\left.+\alpha^2\left\{\sum_E\left(\frac{\varepsilon}{\varepsilon_y}\right)\xi^2+\sum_P\mathrm{sgn}\left(\frac{\varepsilon}{\varepsilon_y}\right)\xi^2\right\}\right]=1.0-\frac{6}{(1+\beta+\beta^2)}\bar{\nu}\varepsilon_y(\gamma_1+\alpha^2\gamma_2) \tag{8c}$$

In Eqs. 8, $\sum_{Eu}$ indicates the sum of the elastic small rectangular elements of the upper flange and $\sum_{El}$ indicates for the lower flanges, $\bar{\nu}=E/G$, the ratio of the Young's modulus to the shear modulus of elasticity; and $\alpha=b/d$, the ratio of the flange width to the depth of a cross section. Furthermore, $\eta_o d$ is the coordinate of the shear center of the elastic core on the y axis given by

$$\eta_o=\frac{\sum_E\xi^2\eta}{\sum_E\xi^2} \tag{9}$$

From Eq. 4 and Eqs. 8 and 9, the relationships between κ_{iy}, κ_{iw}, κ_{kt} and η_o in the inelastic range and M/M_y can be obtained under given residual stress level and pattern.

It can be observed from numerical calculations that these values are almost independent on β.

Analytical Method

The transfer matrix method in Ref. 15 may be applied in the analysis. Using the state vector given in Appendix, the 8×8 field transfer matrix can be formulated by the nondimensionalized forms which are independent on α.

For the calculation of the tapered beams, the point transfer matrix can be available at the nodal point and two parameters k_b and k_d are introduced which indicate the ratios of the flange width and the depth of a cross section at an arbitrary location to those at the reference point on a beam. The state vectors of both sides at nodal point i can be related by the point matrix given in Appendix which is independent on α and β.

The beam is divided by finite elements and it is assumed that the bending moment at the midpoint of an element is uniformly distributed in the element. Furthermore, for the tapered beams, it is assumed that the cross section is constant in an element and its dimension is represented by that at the midpoint of the element. Using the reduction factors and the sectional constants corresponding to the nondimensionalized bending moment by M_y and premultiplying the field transfer matrix of each element from left end to right, the state vectors at left and right ends can be related with each other. The buckling conditions in this case can be given by

$$|\mathbf{R}'\mathbf{F}_n\mathbf{P}_{n-1}\mathbf{F}_{n-1}\mathbf{P}_{n-2}\cdots\mathbf{P}_2\mathbf{F}_2\mathbf{P}_1\mathbf{F}_1\mathbf{R}| = 0 \tag{10}$$

in which $\mathbf{F}_1$, $\mathbf{F}_2$, $\cdots$ $\mathbf{F}_n$ = the field transfer matrices of elements 1, 2, $\cdots n$; $\mathbf{P}_1$, $\mathbf{P}_2$, $\cdots$ $\mathbf{P}_{n-1}$ = the point transfer matrices at nodes 1, 2, $\cdots$ $n-1$ and $\mathbf{R}$, $\mathbf{R}'$ = the boundary matrices at left and right ends. The critical moment may be determined as the smallest root of this determinantal equation.

Based upon this formulated equation, a computer program was developed to provide numerical results by trial and error procedure. First, the bending moment at the midpoint of each element is calculated for an arbitrary critical load factor then the reduction factors corresponding to the bending moment are numerically evaluated for each element. Second, the determinant of Eq. 10 is calculated. The calculation of these steps must be repeated using a new value of the critical load factor until a sufficient accuracy is obtained.

Buckling Strength under Pure Bending

Effects of Geometrical Shapes and Residual Stresses

As the factors to affect the lateral buckling strength of plate girders under pure bending, the ratio of the web height to the depth of a cross section, $\beta = d_w/d$, the magnitudes of a residual stress and the yield strain may be considerable from above discussion.

The nondimensionalized field transfer matrix discussed above is only a function of β as far as the dimensions of a cross sectional geometry are concerned and α is only

included in the coefficient of the equivalent St. Venant torsional rigidity given in Eq. 8c. But because γ_2 in Eq. 8c is considerably less than γ_1, the effect of α to the coefficient κ_{kt} is sufficiently small for usually used plate girders. For instance, the buckling strengths of $\alpha=0.1$ and 0.5 were compared for $\sigma_{rc}=0.3\sigma_y$ and $\varepsilon_y=0.0012$. From the numerical results, the difference between two cases is less than 1% in the elastic range and decreases further in the inelastic range. Thus, $\alpha=0.3$ may be used in the following numerical calculations.

Fig. 3 shows the effects of three magnitudes of the residual stress, $\sigma_{rc}=0.1\sigma_y$, $0.3\sigma_y$ and $0.5\sigma_y$, to the lateral buckling strength for three values of $1/\beta=1.03$, 1.05 and 1.07. The vertical line indicates M/M_y and the horizontal line indicates L/b. The boundary conditions are simply supported for the lateral displacement and the rotation at both ends and $\varepsilon_y=0.0012$ is used. From the figure, the buckling strength is greately affected by the parameter β in the elastic range but that effect decreases in the inelastic range with the reduction of L/b.

The elastic buckling moment of a doubly symmetric I-shaped beam without residual stress under pure bending can be expressed by [3],

$$(M_o)^e_{cr}=\frac{\pi}{L}\sqrt{EI_yGK_T\left(1+\frac{\pi^2EI_w}{GK_TL^2}\right)} \tag{11}$$

Substituting Eqs. 5, 6 and using Eqs. 7 and unity for κ_{iy}, κ_{iw}, κ_{kt}, the non-dimensionalized critical moment by the yield moment, $(m_o)^e_{cr}$ can be obtained by

$$(m_o)^e_{cr}=\frac{\pi}{2\sqrt{2(1+\nu)\varepsilon_y}}\frac{(1-\beta)^2}{(1-\beta^3)}\left(\frac{b}{L}\right)\sqrt{1+\tfrac{1}{8}(1+\nu)\pi^2\frac{(1+\beta)^2}{(1-\beta)^2}\left(\frac{b}{L}\right)^2} \tag{12}$$

in which $\nu=$ Poisson's ratio.

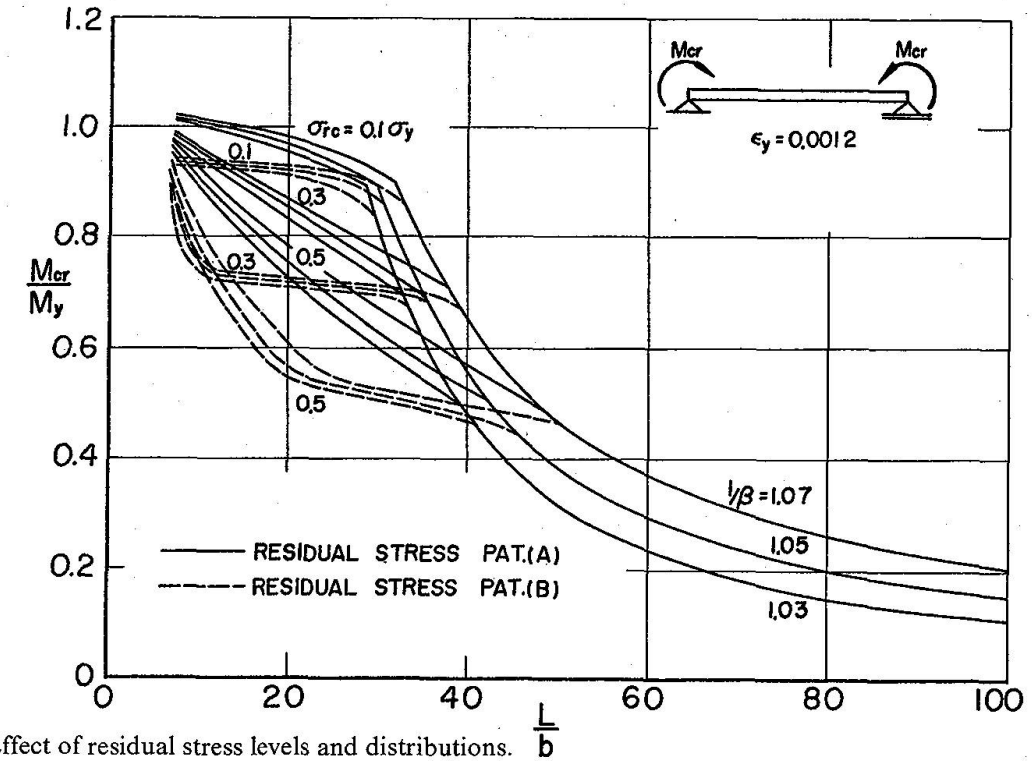

Fig. 3. Effect of residual stress levels and distributions.

Taking the vertical line the quotient of the nondimensionalized critical moment, M_{cr}/M_y, divided by $(m_o)^e_{cr}$ and the horizontal line the reciprocal of the square root of $(m_o)^e_{cr}$,

$$\lambda = 1/\sqrt{(m_o)^e_{cr}} \tag{13}$$

the buckling curves in the elastic range are horizontaly straight and these values are slightly less than unity because the residual stress reduces the elastic buckling strength.

The curves are independent on the geometrical shapes of the cross section but slightly depend on the residual stress levels and distributions. Thus, in this representation, the starting point of an inelastic buckling curve is independent on the geometrical shapes of the cross section. Fig. 4 shows the same buckling curves as Fig. 3 represented by such manner for the residual stress patterns (*A*) and (*B*), respectively. Fig. 5 shows the difference between both the residual stress patterns (*A*) and (*B*) for $\sigma_{rc}=0.3\sigma_y$.

In these figures, the solid curves and the dotted curves indicate for $1/\beta = 1.03$ and 1.07, respectively. It can be observed that the curves are also independent on the geometric dimensions and only depend on the residual stress levels and distributions in the inelastic range.

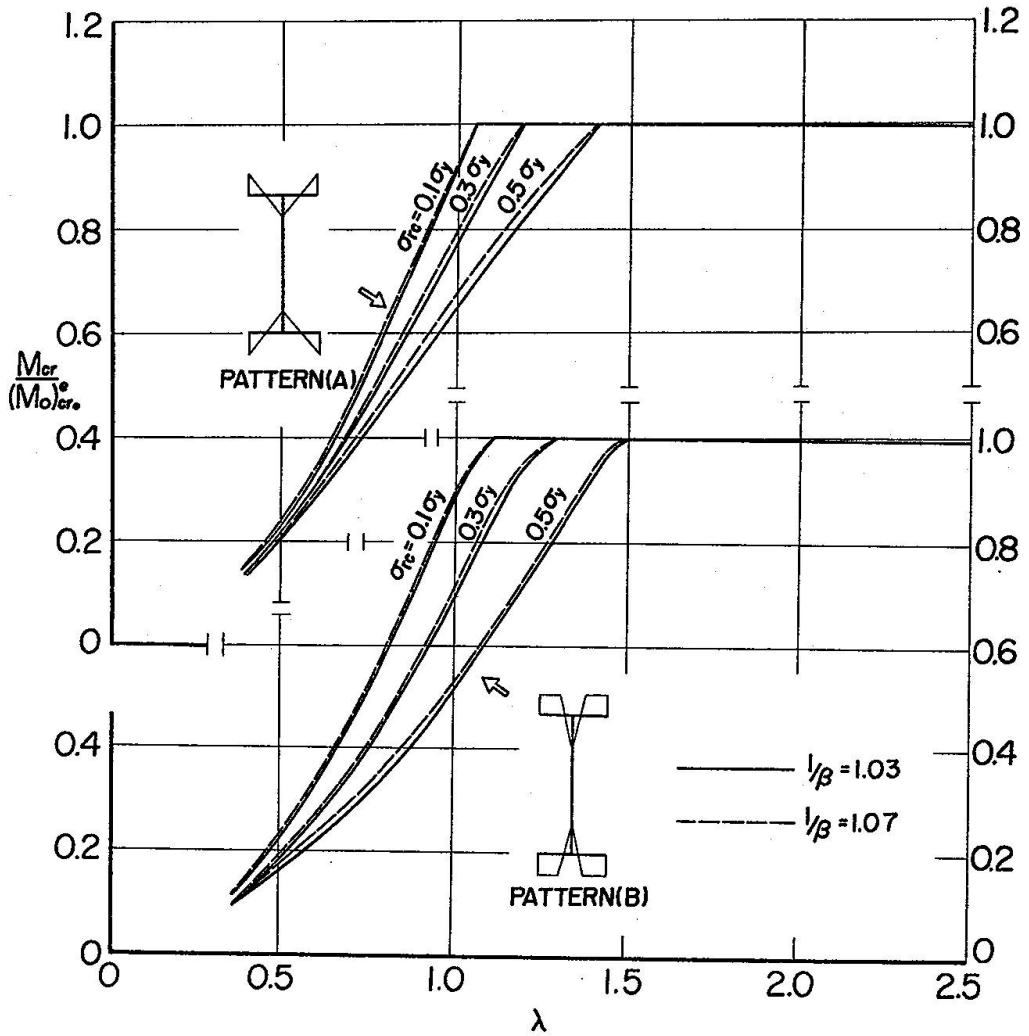

Fig. 4. A possible representation of buckling curves.

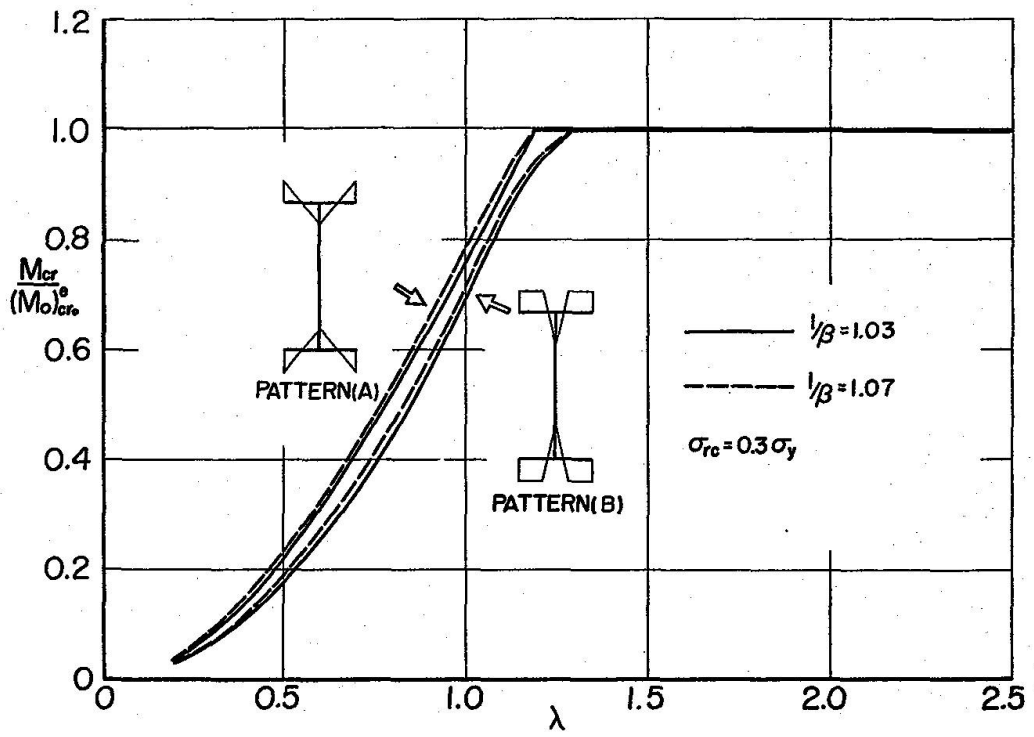

Fig. 5. Comparison between residual stress patterns.

Effect of the St. Venant Torsional Stiffness

It has been proposed that the lateral buckling strength calculated by neglecting the St. Venant torsional stiffness may be used for the plate girders with the relative short buckling length braced by cross beams or lateral bracings [1]. From this view point, both buckling curves for a uniform bending considering and neglecting the St. Venant torsional stiffness are compared in Fig. 6 by thick curves and thin curves, respectively.

The vertical line indicates the nondimensionalized critical bending moment, M_{cr}/M_y, and the horizontal line indicates the span length divided by the flange width, L/b.

The solid curves are for the residual stress pattern (A) and the dotted curves for the pattern (B) and $\sigma_{rc}=0.3\sigma_y$, $\varepsilon_y=0.0012$ are used. The values neglecting the St. Venant torsional stiffness are independent on the values of β in a long span length but slightly depend upon β in a relatively short span length.

The difference between the values considered and neglected the St. Venant torsional stiffness is small for $1/\beta=1.03$ but the strength calculated by neglecting the St. Venant torsional stiffness is on the safe side for $1/\beta=1.07$.

Effect of the Yield Stress Levels

The buckling curves in Fig. 3 are for the yield strain $\varepsilon_y=0.0012$. However, in the nondimensionalized representation of the buckling curves as Figs. 4 and 5, the effect of the yield strain will disappear because the yield strain only affects κ_{kt} and the influence on it is negligible.

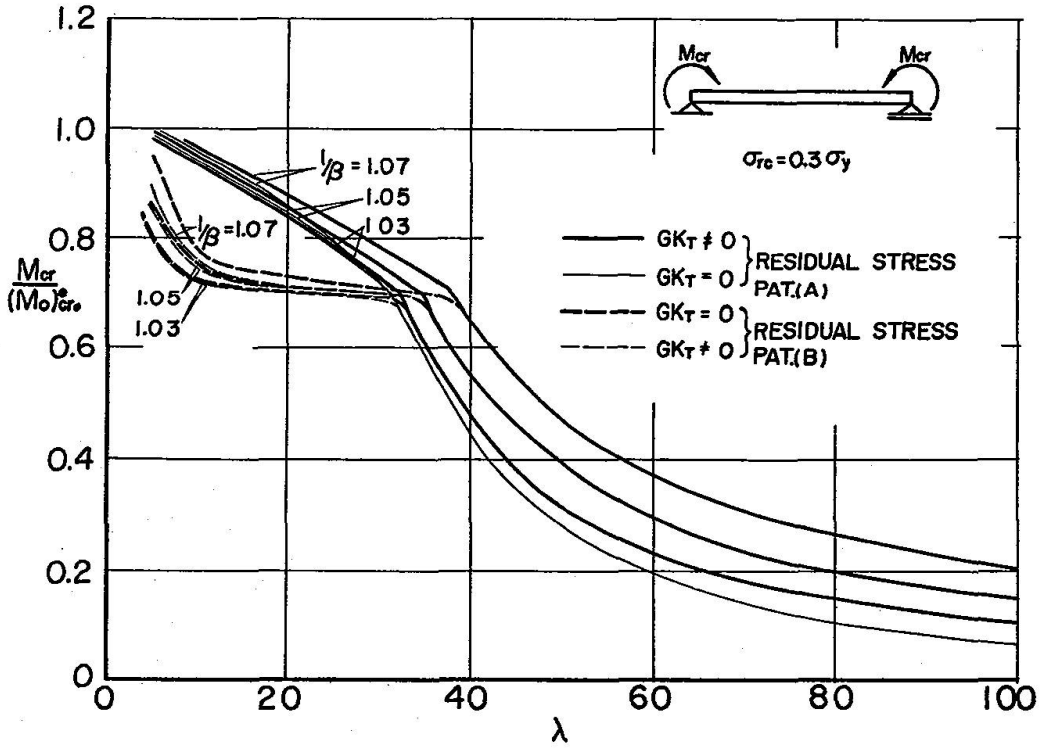

Fig. 6. Effect of St. Venant torsional stiffness.

Comparison with Test Results

In Ref. 2, Fukumoto *et al.* have carried out the tests of the plate girders. The experiments under the pure bending consisted of thirty-seven welded built-up beams and girders made from *SM*50 (*A*441) or *HT*80 (*A*514) steel. Some of them are annealed. The boundary conditions are fixed for the lateral displacements and the rotations at both ends.

The experimental values are plotted in Fig. 7. The vertical line indicates the nondimensionalized bending moment, $M_{cr}/(M_o^F)_{cr}^e$ and the horizontal line indicates $\lambda_F = 1/\sqrt{(M_o^F)_{cr}^e/M_y} = 1/\sqrt{(m_o^F)_{cr}^e}$ in which $(M_o^F)_{cr}^e$ = the elastic critical bending moment of the plate girder without the residual stress under the pure bending of which boundary conditions are fixed for the lateral displacements and the rotations at both ends. In the figure, the theoretical values are also shown by solid curve, dotted curve and one-dotted curve for plate girders without residual stress, with residual stress patterns (*A*) and (*B*) for $\sigma_{rc}=0.3\ \sigma_y$, respectively. In the representation, the effect of the geometrical shapes and the yield stress levels may not be included and only the effect of the residual stress levels and distributions is included.

The experimental results scatter in a relative small range and the theoretical curves for the residual stress pattern (*B*) with $\sigma_{rc}=0.3\sigma_y$ may give the lower bound.

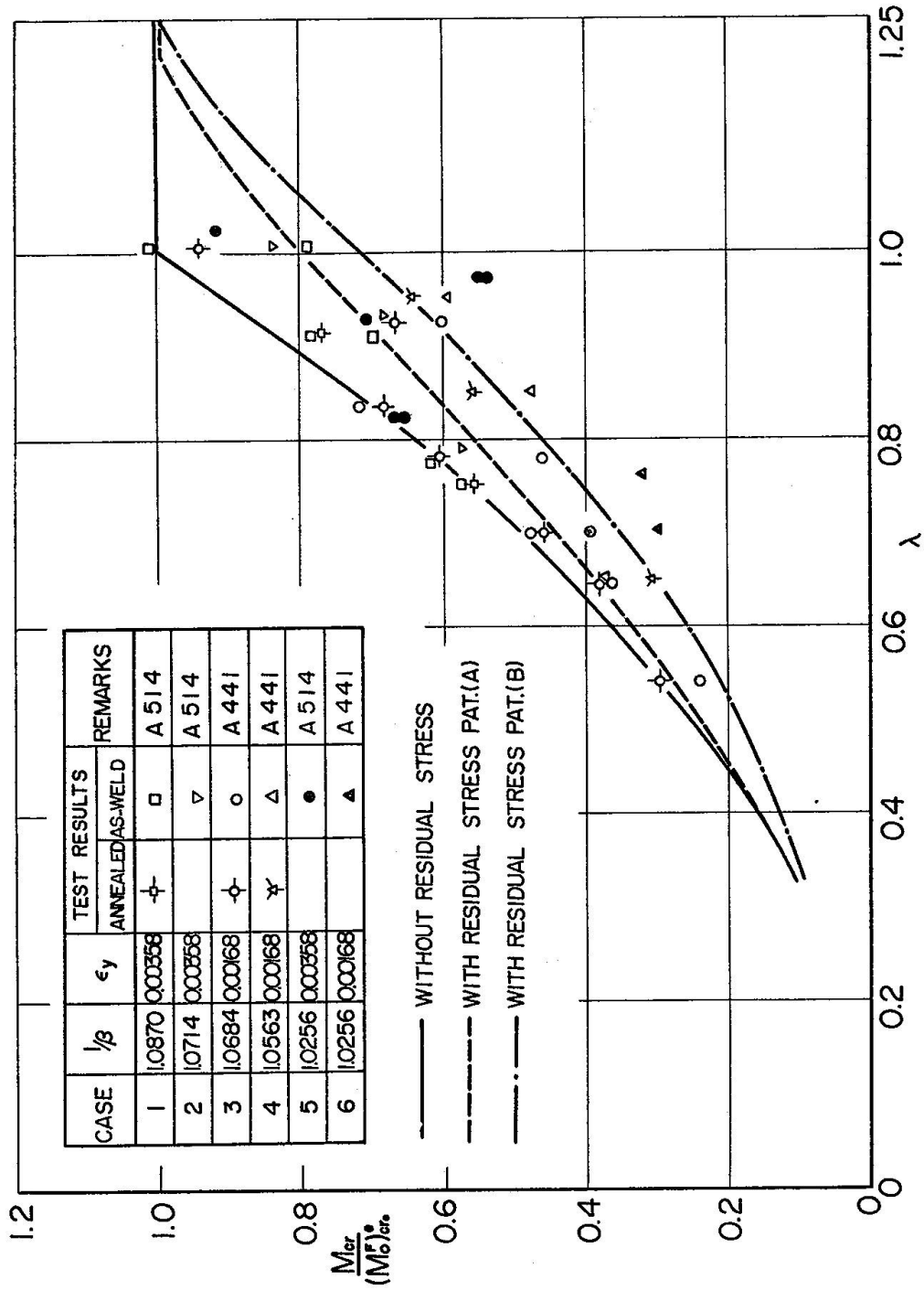

Fig. 7. Comparison with experimental results.

Buckling Strength under Various Loading Conditions

Fig. 8 shows the lateral buckling curves under three loading cases for $\sigma_{rc} = 0.3\sigma_y$. A uniform bending moment, a concentrated load applied at the midspan and a uniformly distributed load are considered. The uniform moment may be the most severe loading condition for the lateral buckling, the concentrated load at the midspan may be the most lenient condition and the uniformly distributed load lies midway.

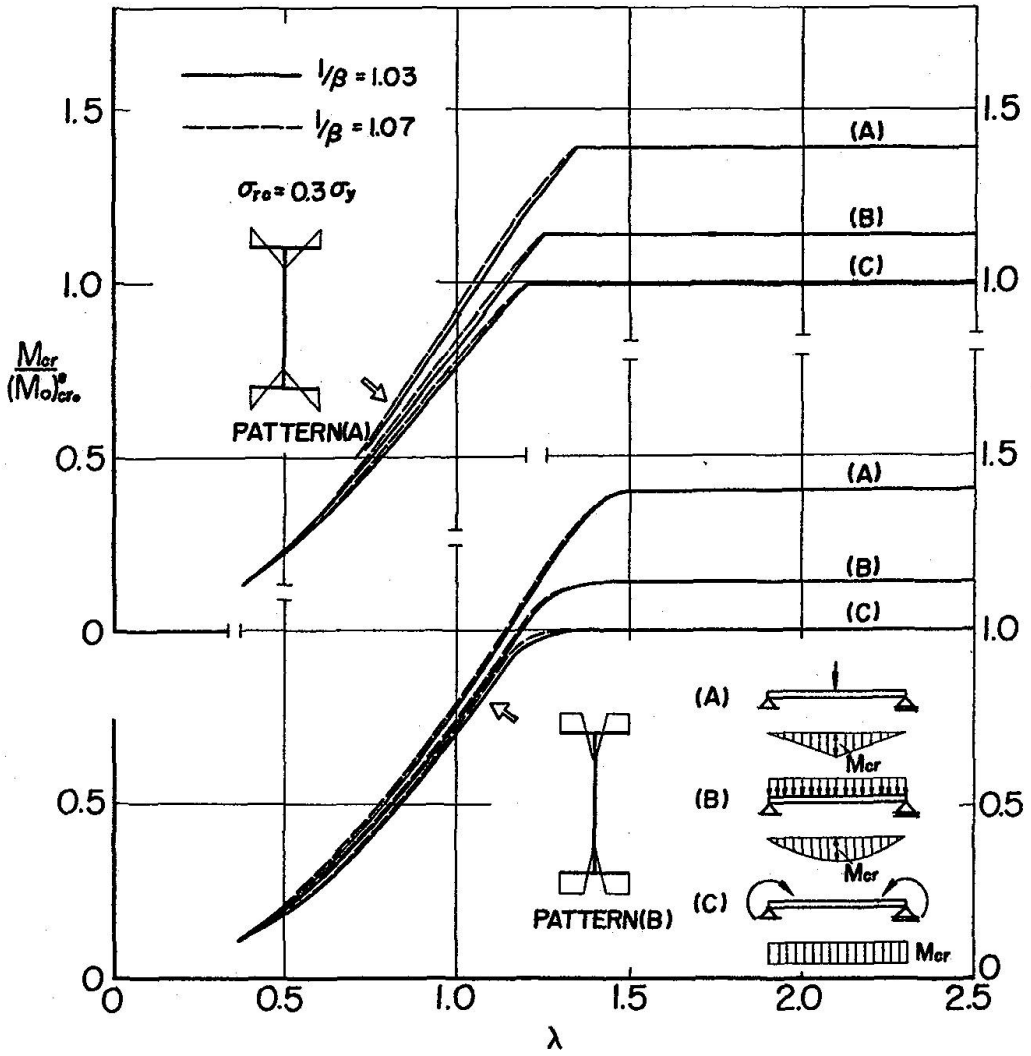

Fig. 8. Buckling curves for various loading conditions.

The horizontal line indicates λ given by Eq. 13 and the vertical line indicates the quotient of the nondimensionalized bending moment at the midspan corresponding to the buckling load, M_{cr}/M_y, divided by the elastic critical moment given by Eq. 12.

The effect of β to the buckling curves can be observed little in the elastic and the inelastic ranges for both the residual stress patterns.

Buckling Strength of Tapered Plate Girders

Effect of Variations of Cross Section and Loading Conditions

Three types of the variation of cross sections along the span length are considered. 1. The flange widths or depths of the cross section decrease linearly from the midspan (Type A); 2. remain a constant at a central one-third of the span length and decrease linearly at both outside one-thirds (Type B), and 3. decrease parabolically from the midspan (Type C).

For each type of the variation, the buckling strength under three loading cases of a uniform moment, a concentrated load at the midspan and a uniformly distributed load is calculated. The boundary conditions are simply supported for the lateral displacements and the rotations at both ends.

A few numerical examples are shown in Figs. 9 and 10. Fig. 9 shows the buckling curves for a concentrated loading case under a constant depth of the cross section, $k_d = 1.0$ and $/\beta = 1.05$. Only the flange widths vary such that the ratios of the flange width at the ends of the plate girder to that at the reference point of the midspan, k_{bo}, decrease from 1.0 to 0.2 with 0.2 pitch. The vertical line indicates the ratio of the nondimensionalized critical moment at the midspan, $M_{cr}/(M_y)_o$, for the varying cross section to the elastic critical moment, $(m_o)^e_{cro}$, in which $(M_y)_o$ and $(m_o)^e_{cro}$ are the yield moment and the elastic critical moment given in Eq. 12 for the uniform cross section of which dimensions are at the midspan of the varying cross section. The horizontal line indicates $\lambda_o = 1/\sqrt{(m_o)^e_{cro}}$ and the solid, dotted and one-dotted curves show for the types A, B and C, respectively.

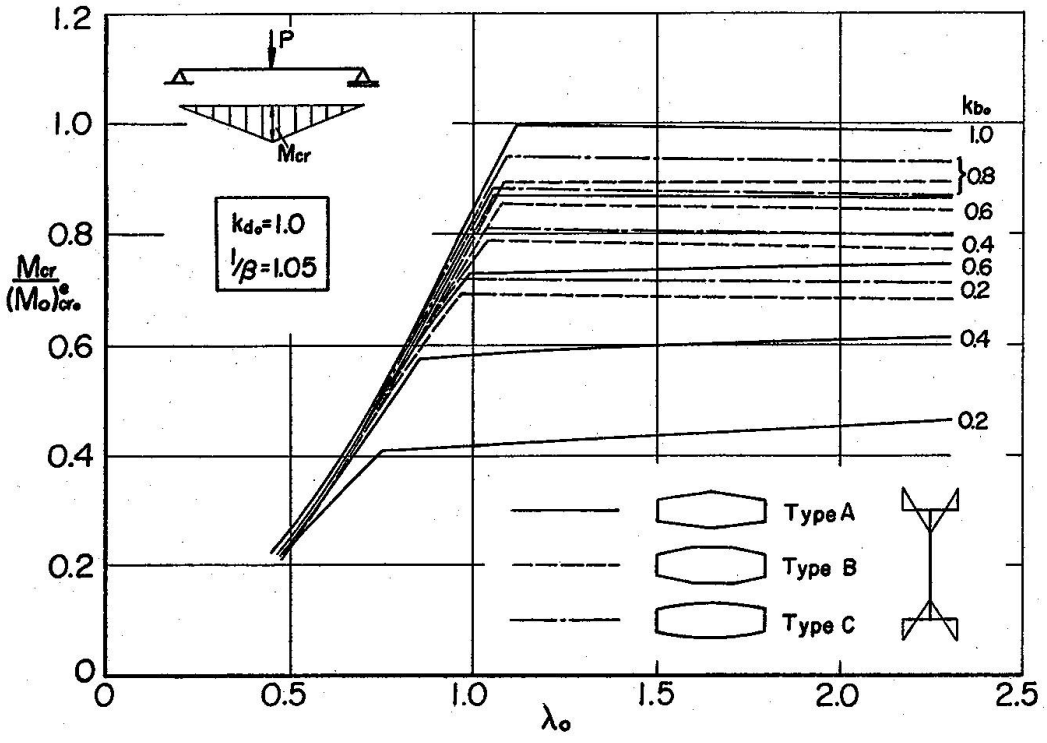

Fig. 9. Buckling curves of plate girders with tapering flange widths.

Fig. 10 shows the buckling curves under the same conditions except the depth of the cross section varies and the flange widths and $1/\beta$ remain constants. When the depths of the cross section and $1/\beta$ remain constants, the curves in the elastic range in Fig. 9 are almost straight and keep constants except for small values of k_{bo} of Type A but in the inelastic range, the curves decrease parabolically with the reduction of λ_o. When the widths of the flange and $1/\beta$ remain constants, the curves in the elastic range in Fig. 10 are ascending with the reduction of λ_o and this tendency becomes remarkable with the degree of taper. In the inelastic range, the curves decrease parabolically with the reduction of λ_o. From the numerical calculations, the buckling curves in Figs. 9 and 10 are independent on the values of β in both the elastic and the inelastic ranges when the value of β keeps a constant along the whole length of the plate girders. For other cases of the loading, the same tendency can be observed in the elastic and the inelastic ranges.

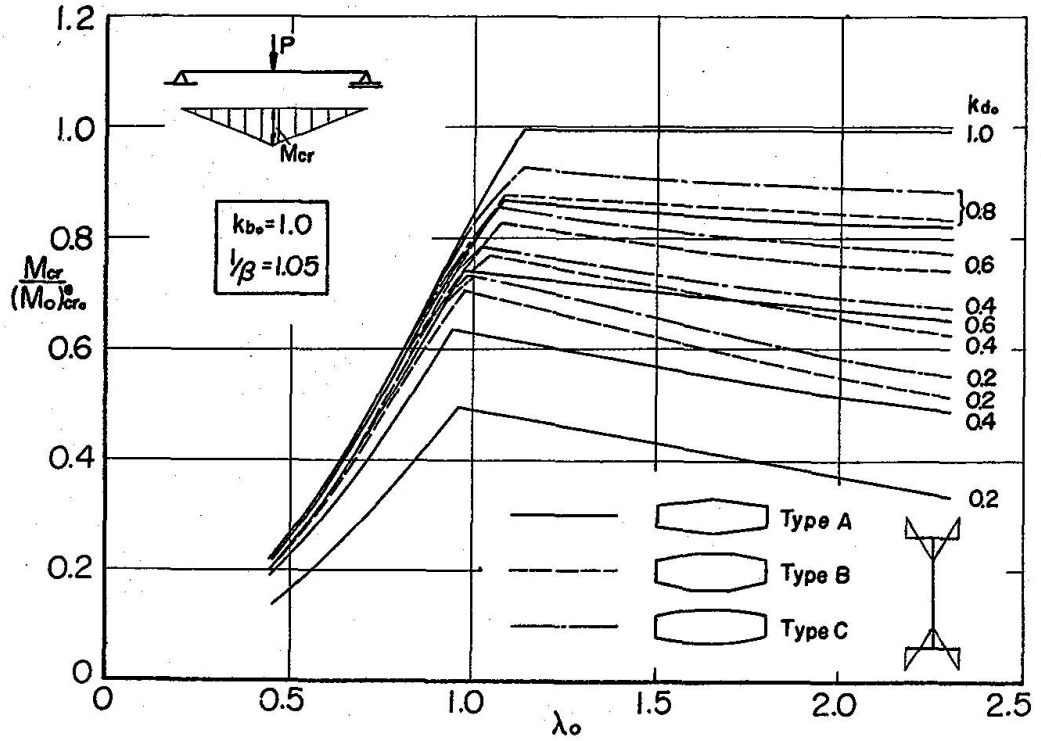

Fig. 10. Buckling curves of plate girders with tapering web depths.

Design Approximations for Plate Girders with Tapering Flange Widths or Web Depths

It is assumed that the flange widths or the web depths are linearly tapered between the restricted points of a plate girder by cross beams or lateral bracings and at these points the plate girder is simply supported for the lateral displacements and the rotations. The cross sectional dimensions of the plate girders are usually designed such that the stresses go near the margine under a applying bending moment. Thus, the bending moments at the restricted points in the plate girder may be proportional to the yield moments or the full plastic moments of the cross sections.

In the numerical calculations, it is assumed in addition to above assumptions that the bending moments at the restricted points are proportional to the yield moments of the cross sections and the bending moment distribution is linear between these points.

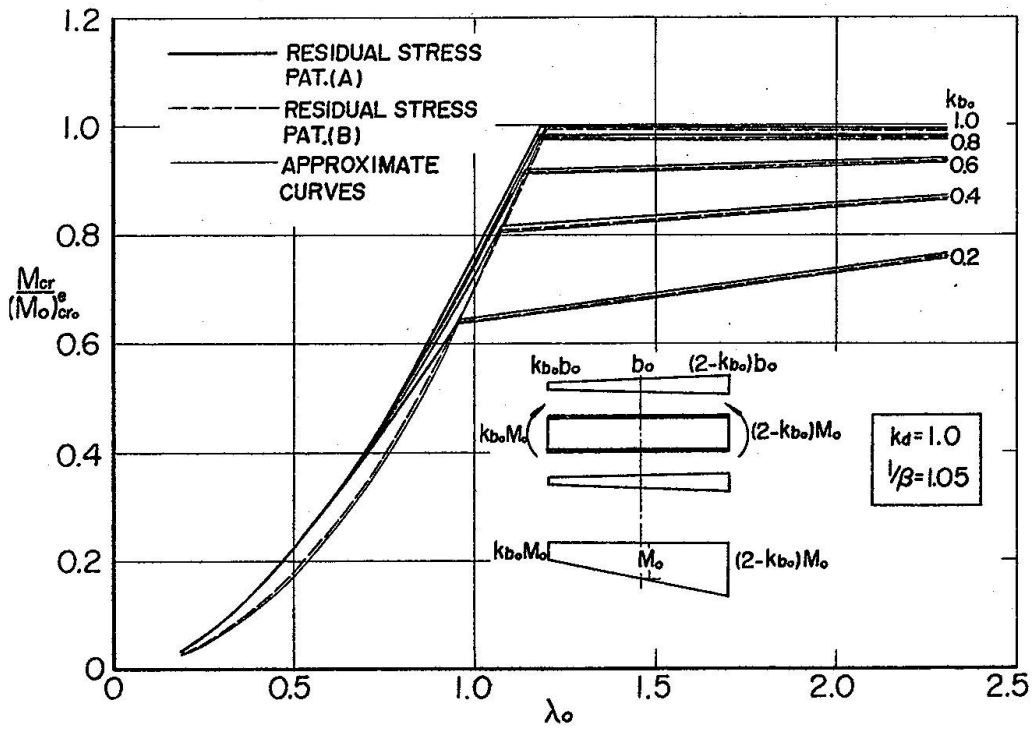

Fig. 11. Buckling curves of plate girders with linearly tapered flange widths.

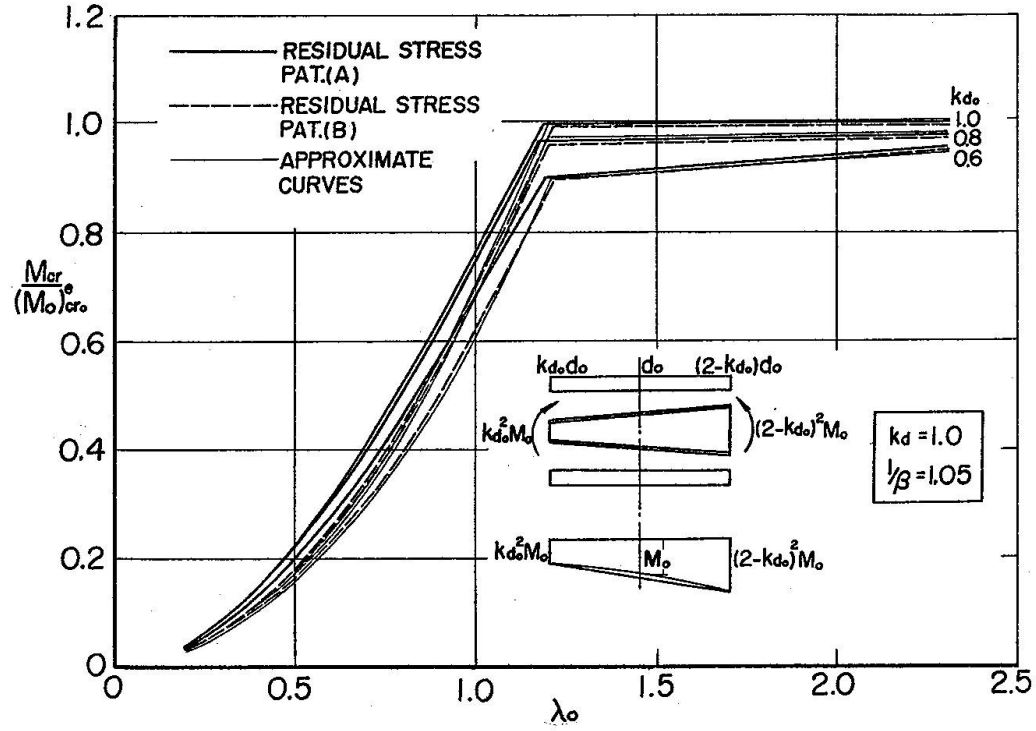

Fig. 12. Buckling curves of plate girders with linearly tapered web depths.

Fig. 11 shows the buckling curves of the plate girders with linearly tapering flange widths. The horizontal line indicates λ_o and the vertical line indicates the critical moment at the midspan nondimensionalized by the same manner as Figs. 9 and 10.

The degrees of the taper of the flange widths, k_{bo}, are the ratios of the smaller flange width at the supports to the flange width at the midspan. In the numerical calculations, $1/\beta = 1.05$ is used and the buckling curves in the figures are shown by solid curves for the residual stress pattern (A) and by dotted curves for the pattern (B). The same illustration for the plate girders with linearly tapering web depth is given in Fig. 12. It should be noted that the yield moment of the cross section is not vary linearly along a span in this case.

The curves in the elastic ranges in Figs. 11 and 12 are almost straight and keep constants under a gentle taper of cross sections. However, when the degrees of taper become steep, the curves are descending with the reduction of λ_o. In the inelastic range, the curves decrease parabolically with the reduction of λ_o.

The discrepancy between the buckling curves in Fig. 11 or 12 for $1/\beta = 1.05$ and for the values of $1/\beta = 1.03$ or 1.07 cannot be recognized.

In the figures, the thin lines show the approximate design formulae proposed herein by

$$\frac{M_{cr}}{(M_o)^e_{cro}} = C_1 + (1.0 - C_1)\,(2.0 - k)k \tag{14}$$

in the elastic range and

$$\frac{M_{cr}}{(M_o)^e_{cro}} = C_2\lambda_o^2 \tag{15}$$

in the inelastic range in which $C_1 = 0.15\lambda_o + 0.3$ and $C_2 = 0.7$ for the tapering flange widths and $C_1 = 0.3\lambda_o$, $C_2 = 0.7 - 0.5 \times (1.0 - k_{do})^2$ for tapering web depths, respectively and k is the degree of the taper of flange width or web depth.

Remarks on Practical Application

In this paper, the effects to the rigidities of the web of plate girders were neglected in the analysis. It is well known that the model neglected the effects of web gives a good approximation to the lateral flexural and the warping rigidities. However, the error accompanied by the calculation of the axial forces of the flanges may not be small. A few actual plate girders were examined considering and neglacting the web effects in this view point. As the result, it is found that the representation of the buckling curves as shown in Fig. 4 gave a satisfactory agreement for both cases.

The buckling strength of the plate girders with tapering flange wides or web depths decreases comparing the strength of those with a uniform cross section for all loading conditions of a uniform bending moment, a concentrated load and a uniformly distributed load. The economy of the flange or the web weight of the plate girders with tapering constant k_{bo} or k_{do} can be given by $(1-k)/2$ and $(1-k)/3$ for the Type A and Type B, C, respectively, in which k = a tapering constant k_{bo} or k_{do}.

The reduction of the buckling strength of plate girders with a tapering cross section exceeds the decrease of the flange or the web weight in the elastic range. This tendency is most remarkable under a loading case of a uniform bending moment and least under a concentrated loading case. However, in the inelastic range, the reduction of the strength can not be almost recognized under both the cases of a concentrated load and a uniformly distributed load.

The results shown in Figs. 11 and 12 may contribute to the rational design of plate girders.

Conclusions

The elastic and the inelastic lateral buckling strength of I-shaped plate girders were studied theoretically and a general method of analysis was developed by the transfer matrix method in the nondimensional form. First, it was shown that the sectional properties in the inelastic range could be calculated numerically by only β as a parameter of cross sectional dimensions. Secondly, the field transfer matrix was derived in the nondimensional form and the point transfer matrix which took the variation of the cross section into account was expressed.

A new representation of the buckling curves which was independent on the cross sectional geometry of plate girders and only depend on the residual stress levels and distributions. Using this representation, the numerical examples were presented for the simply supported plate girders with uniform and tapered cross sections under various loading conditions. It was also shown that the experimental results could be adjusted by this method.

The method should find a particular application in the design of plate girders.

Appendix - Transfer Matrices

State Vector

Using the same notations as in Ref. 15, the following nondimensionalized state vector may be used.

$$V = \left\{\frac{u}{b}\ \theta\ \frac{\phi}{\alpha}\ \frac{\rho b}{\alpha}\ \frac{S}{\alpha\sigma_y d^2}\ \frac{M_\eta}{\alpha^2\sigma_y d^3}\ \frac{M_z}{\alpha\sigma_y d^3}\ \frac{M_w}{\alpha^2\sigma_y d^4}\right\} \tag{16}$$

in which u and θ = the lateral displacement and its slope at shear center; ϕ = the angle of twist; ρ = the angle of twist per unit length; S = the lateral shear force; M_η = the bending moment about weak axis; M_z = the torsional moment and M_w = the bimoment produced by warping.

Point Transfer Matrix

The compatibility and the equilibrium conditions at the nodal point i where the cross section is discontinuous are obtained as follows [14] considering the movement of the locations of shear center:

$$
\begin{aligned}
u_i^L &= u_i^R - \Delta s \phi_i^R \\
\theta_i^L &= \theta_i^R - \Delta s \rho_i^R \\
\phi_i^L &= \theta_i^R \\
\rho_i^L &= \rho_i^R \\
S_i^L &= S_i^R \\
M_{\eta i}^L &= M_{\eta i}^R \\
M_{zi}^L &= M_{zi}^R - \Delta s (m_{oi}^R M_{yi}^R \rho_i^R - S_i^R) \\
M_{wi}^L &= M_{wi}^R + \Delta s M_{\eta i}^R
\end{aligned} \tag{17}
$$

in which Δs = the movement of the shear center downward.

The elements of the 8×8 point transfer matrix can be expressed by the non-dimensional form as follows:

$$
\begin{aligned}
(1,1) &= \left(\frac{k_b^L}{k_b^R}\right) & (1,3) &= \Delta\eta\left(\frac{k_b^L}{k_b^R}\right) \\
(2,2) &= 1.0 & (2,4) &= \Delta\eta \\
(3,3) &= \left(\frac{k_b^L}{k_b^R}\right)\left(\frac{k_d^R}{k_d^L}\right) & (4,4) &= \left(\frac{k_d^R}{k_d^L}\right) \\
(5,5) &= \left(\frac{k_b^L}{k_b^R}\right)\left(\frac{k_d^L}{k_d^R}\right) & (6,6) &= \left(\frac{k_b^L}{k_b^R}\right)^2\left(\frac{k_d^L}{k_d^R}\right) \\
(7,4) &= m_o \mu_s \Delta\eta\left(\frac{k_b^L}{k_b^R}\right)\left(\frac{k_d^L}{k_d^R}\right)^2 & (7,5) &= -\Delta\eta\left(\frac{k_b^L}{k_b^R}\right)\left(\frac{k_d^L}{k_d^R}\right)^2 \\
(7,7) &= \left(\frac{k_b^L}{k_b^R}\right)\left(\frac{k_d^L}{k_d^R}\right)^2 & (8,6) &= \Delta\eta\left(\frac{k_b^L}{k_b^R}\right)^2\left(\frac{k_d^L}{k_d^R}\right)^2 \\
(8,8) &= \left(\frac{k_b^L}{k_b^R}\right)^2\left(\frac{k_d^L}{k_d^R}\right)^2
\end{aligned}
$$

in which $\Delta\eta = \eta_o^R(k_d^R/k_d^L) - \eta_o^L$; η_o^L, η_o^R = the values of η_o on the left and the right side elements at point i and k_b^L, k_d^L, k_b^R, k_d^R = the values of k_b and k_d on the left and the right side elements at point i, respectively.

The unspecified elements are equal to zero.

Notation

The following symbols are used in this paper:

a	distance between point on cross section and shear center.
b	flange width.
d	depth of plate girder.
d_w	web height.
E	Young's modulus of elasticity.
F	field transfert matrix.
G	modulus of elasticity in shear.
GK_T	St. Venant torsional stiffness.
$G\overline{K}_T$	equivalent St. Venant torsional stiffness defined by $GK_T + \overline{K}$.

I_w warping moment of inertia.
I_y moment of inertia about weak axis.
K $\int \sigma a^2 dA$.
k_b, k_d ratios of flange width and depth of plate girder at arbitrary point to those at reference point.
k_{bo}, k_{do} ratios of flange width and depth of plate girder at ends to those at reference point.
L span length.
M bending moment.
M_{cr} critical moment.
M_y yield moment of cross section without residual stress.
M_w bimoment produced by warping.
M_z torsional moment.
M_η bending moment about weak axis.
M_o bending moment at midpoint of element.
$(M_y)_o$ yield moment of cross section without residual stress at reference point.
$(M_o)^e_{cr}$ elastic critical moment of simply supported beam under pure bending.
$(M^F_o)^e_{cr}$ elastic critical moment of fixed beam under pure bending.
$(M_o)^e_{cro}$ elastic critical moment of tapered beam under pure bending.
$(m_o)^e_{cr}$ $(M_o)^e_{cr}/M_y$.
$(m^F_o)^e_{cr}$ $(M^F_o)^e_{cr}/M_y$.
$(m_o)^e_{cro}$ $(M_o)^e_{cro}/(M_y)_o$.
m, n dividing number of flange thickness and width.
P point transfer matrix.
R, R' Boundary matrices at left and right ends.
S section modulus.
lateral shear force.
t flange thickness.
u lateral displacement.
w web thickness.
α ratio of flange width to depth of plate girder, $\alpha = b/d$.
β ratio of web height to depth of plate girder, $\beta = d_w/d$.
γ_1, γ_2 sectional constants in inelastic range defined in Eq. 8 c.
Δs movement of shear center.
ε strain at point on cross section.
ε_r residual strain.
ε_y yield strain.
ε_ϕ strain due to bending.
ε_o uniform strain on cross section.
ηd distance from x axis to point on cross section.
$\eta_o d$ distance from x axis to shear center.
θ slope of lateral displacement.
κ reduction factor (subscripts *kt, iw* and *iy* denote K_T, I_w and I_y).
μ coefficient defined by Eqs. 7 (subscripts *kt, s, iw* and *iy* denote K_T, S, I_w *and* I_y).
λ $1/\sqrt{(m_o)^e_{cr}}$

λ_F $1/\sqrt{(m_o^F)_{cr}^e}$.

λ_o $1/\sqrt{(m_o)_{cro}^e}$.

ν Poisson's ratio.

$\bar{\nu}$ E/G.

ξb distance from y axis to point on cross section.

ρ angle of twist per unit length.

σ stress on cross section.

σ_{rc}, σ_{rt} residual compressive and tensile stresses.

σ_y yield-stress level.

ϕ curvature.

angle of twist.

ϕ_y curvature corresponding to first yield in flexure.

Acknowledgments

The writer is grateful to Fumio Nishino of the University of Tokyo and Yuhshi Fukumoto of Nagoya University for their valuable suggestions. He wish to record also his appreciation to Haruko Kitada and Yutaka Hosokawa for their assistance. The numerical calculations were carried out by HITAC 8700/8800 in the University of Tokyo and FACOM 230-35 in Kanazawa University.

References

1. Column Research Council: Guide to Design Criteria for Metal Compression Members. 2nd ed., Ed. B.G. Johnston, John Wiley and Sons, New York, 1966.
2. FUKUMOTO, Y., FUJIWARA, M., and WATANABE, N.: Ineslastic Lateral Buckling Tests on Welded Beams and Girders (in Japanese). Proceedings, Japan Society of Civil Engineers, No. 189, May, 1971, pp. 39-51.
3. GALAMBOS, T.V.: Structural Members and Frames. Prentice-Hall Book Co., Englewood Cliffs, N.J., 1968.
4. GALAMBOS, T.V.: Inelastic Lateral Buckling of Beams. Journal of the Structural Division, ASCE, Vol. 89, No. ST5, Proc. Paper 3683, Oct., 1963, pp. 217–242.
5. HAMAYOSHI, F.: On Torsion of I-Beam with a Web of Variable Height. Memoir, Faculty of Engineering, Hokkaido University, Japan, Vol. 11, No. 2, 1961, pp. 209–228.
6. KITIPORNCHAI, S., and TRAHAIR, N.S.: Elastic Stability of Tapered I-Beams. Journal of the Structural Division, ASCE, Vol. 98, No. ST3, Proc. Paper 8775, Mar., 1972, pp. 713–728.
7. LEE, G.C., and SZABO, B.A.: Torsional Response of Tapered I-Girders, Journal of the Structural Division, ASCE, Vol. 93, No. ST5, Proc. Paper 5505, Oct., 1967; pp. 233–252.
8. LEE, L.H.N.: Non-Uniform Torsion of Tapered I-Beams. Journal of the Franklin Institute, Vol. 262, 1956, pp. 37–44.
9. LEE, L.H.N.: On the Lateral Buckling of a Tapered Narrow Rectangular Beams. Journal of Applied Mechanics, ASME, Vol. 26, Series E, No. 3, Sept., 1959, pp. 457–458.
10. MASSEY, C., and PITMAN, F.S.: Inelastic Lateral Stability Under a Moment Gradient. Journal of the Engineering Mechanics Division, ASCE, Vol. 92, No. EM2, Proc. Paper 4779, Apr. 1966, pp. 101–111.
11. NETHERCOT, D.A.: Factors Affecting the Buckling Stability of Partially Plastic Beams. Proceedings, Institution of Civil Engineers, Part 2, Vol. 53, Proc. Paper 7526, Sept., 1972, pp. 285–304.
12. TRAHAIR, N.S., and KITIPORNCHAI, S.: Elastic Lateral Buckling of Stepped I-Beams. Journal of the Structural Diversion, ASCE, Vol. 97, No. ST10, Proc. Paper 8445, Oct. 1971, pp. 2535–2548.

13. TRAHAIR, N.S., and KITIPORNCHAI, S.: Buckling of Inelastic I-Beams Under Uniform Moment. Journal of the Structural Division, ASCE, Vol. 98, No. ST11, Proc. Paper 9339, Nov. 1972, pp. 2551–2566.
14. UNGER, B.: Elastisches Kippen von beliebig gelagerten und aufgehängten Durchlaufträgern mit einfach-symmetrischem, in Trägerachse veränderlichem Querschnitt unter Verwendung einer Abwandlung des Reduktionsverfahrens als Lösungsmethode. Der Stahlbau, Heft 5, 1970, pp. 135–142, and Heft 6, 1970, pp. 181–184.
15. YOSHIDA, H., and IMOTO, Y.: Inelastic Lateral Buckling of Restrained Beams. Journal of the Engineering Mechanics Division, ASCE, Vol. 99, No. EM2, Proc. Paper 9666, Apr., 1973, pp. 343–366.

Summary

It is shown that the lateral buckling strength of I-shaped plate girders can be expressed by only the ratio of the depth of the cross section to the web height with respect to the cross sectional geometry in both the elastic and inelastic ranges.

Then, the influence of such factors as cross sectional geometry, loading conditions, yield stress levels and residual stress distributions is discussed. Furthermore, the effect of the variations of cross sections with tapering flange widths or web depths is investigated in both the elastic and inelastic ranges.

Résumé

La contrainte critique de déversement de poutres en double té peut s'exprimer, tant dans le domaine élastique que dans le domaine inélastique, à l'aide d'un paramètre de section unique: le rapport de la hauteur totale de la section à la hauteur d'âme. L'auteur envisage de plus l'influence de divers facteurs tels que la forme de la section, les conditions de charge, la valeur de la limite élastique et la répartition des contraintes résiduelles. On étudie enfin, pour les domaines élastique et inélastique, l'effet des variations de sections (largeur des ailes ou hauteur de l'âme variable).

Zusammenfassung

Die kritische Kippspannung eines I-förmigen Trägers lässt sich, sowohl im elastischen als auch im unelastischen Bereich, durch einen einzigen Querschnittsparameter ausdrücken: das Verhältnis der Gesamthöhe des Querschnittes zur Steghöhe. Anschliessend wird der Einfluss der Querschnittsgeometrie, der Belastungsanordnung, der Höhe der Fliessspannung und der Verteilung der Eigenspannungen besprochen, und schliesslich der Einfluss von Querschnittsänderungen (veränderliche Flanschbreite bzw. Steghöhe) im elastischen und unelastischen Bereich.